THE ASTROPHYSICAL JOURNAL, 325:342–354, 1988 February 1

FAST VARIATIONS IN THE ULTRAVIOLET RESONANCE LINES OF α CAMELOPARDALIS (O9.5 Ia): EVIDENCE FOR BLOBS IN THE WIND

HENNY J. G. L. M. LAMERS[1]
Center for Astrophysics and Space Astronomy, University of Colorado; and Joint Institute for Laboratory Astrophysics, University of Colorado and National Bureau of Standards

THEODORE P. SNOW
Center for Astrophysics and Space Astronomy, University of Colorado

AND

CORNELIS DE JAGER AND A. LANGERWERF
SRON Laboratory for Space Research, Utrecht
Received 1987 April 24; accepted 1987 July 27

ABSTRACT

The 72 *IUE* spectra of α Cam and 19 *IUE* spectra of κ Cas, obtained during 72 hours of continuous *IUE* time in 1978 September were searched for variations in the profiles of the resonance lines of Si IV, C IV and N V. No variations were found in the spectra of κ Cas. The UV resonance lines in the spectra of α Cam showed variations at the 2% level near −1800, −700, and +700 km s^{-1}. The first two variations can be explained by absorption components of outward accelerated blobs or shells with an average acceleration of 1.5 cm s^{-2}. The column densities of the blobs or shells are on the order of $N_H \gtrsim 2 \times 10^{20}$ cm^{-2}. If the absorptions are due to blobs with a size of $\sim 1\ R_*$, their mass is $\sim 3 \times 10^{-12}\ M_\odot$. If the absorptions are due to shells, their mass is larger by a factor r_b^2, where r_b is the distance of the shell, which is found to be in the range of $2 \lesssim r_b \lesssim 20\ R_*$. The variation near +700 km s^{-1} can be explained by a variable emission due to a blob which moves away from the star and from the observer and scatters photons in the line of sight. The mass of this blob is at least $2 \times 10^{-10}\ M_\odot$.

The observations suggest that a considerable fraction of the mass of the wind of α Cam, say 10^{-1}, occurs in blobs or shells.

Subject headings: line profiles — mass loss — stars: individual (α Cam) — ultraviolet: spectra

I. INTRODUCTION

Variability is a common characteristic of the winds of early-type stars. This variability is strongest in the UV spectra of Be stars, which can go through cycles of activity with characteristic time scales of the order of decades (e.g., Doazan 1982; Henrichs 1984). The more normal early-type stars also show variations in their UV line profiles.

The discovery of large variations in the UV P Cygni profiles was made by York *et al.* (1977) who found that the O VI lines in the spectrum of δ Ori change by ∼30% in less than 1 hr. The characteristic time for changes in the stellar wind was expected to be of the order of $\tau \sim R_*/v$ which is ∼6 hr if $R_* = 30\ R_\odot$ and $v \approx 1000$ km s^{-1}. The more rapid variations of the O VI lines and the fact that O VI is a superionized species suggested that the source of superionization can change on a shorter time scale than the wind itself.

Subsequent studies of variations in the UV line profiles have shown a different type of variability: the narrow absorption components. Their presence and variability was first discussed by Snow (1977) and the first quantitative interpretation was made by Lamers, Gathier, and Snow (1982), both on the basis of *Copernicus* observations. Since then, numerous studies of the narrow absorption components based on *IUE* observations have been made (see Henrichs 1987 for an excellent review).

The narrow components are variable, both in strength and in radial velocity. If radial velocity variations are observed on a time scale of days or shorter, the components always shift to shorter wavelengths. This suggests that they are produced by matter which is accelerated outward. This matter could be either in shells or in blobs which happen to move in the line of sight toward the star. This distinction between shell ejection or blob-ejection ("puffs") cannot be made on the basis of the variations in the absorption components. However, it is expected that the study of variations over the whole profile might give a clue about the geometry of the ejecta. If the matter is ejected in puffs, one might see a variable absorption if the blobs move in the line of sight toward the stellar disk, and variable emission peaks on either the red or the violet side of the profile by scattering in the blobs if they move outside the line of sight to the stellar disk. On the other hand, if the matter is ejected in shells, one expects to see a variable absorption, combined with a weak emission which is spread out from $-v$ to $+v$ if v is the velocity of the shell.

In an attempt to understand the nature of the variations (puffs or shell ejection) and to determine the frequency of ejection, their mass, and acceleration, we proposed to study the UV spectrum of one supergiant (α Cam O9.5 Ia) in detail during 72 continuous hours in the first year of *IUE* operations. To obtain a maximum amount of information on these variations, an international coordinated campaign was organized for simultaneous studies of this star in the visual (Hα spectroscopy) and in polarimetry. This campaign took place on 1978 September 8–10. A second star (κ Cas, B1 Ia) was added to the campaign. This star, however, did not vary during the observing period (see § II).

In this paper we discuss the variations observed in the UV

[1] Permanent address: SRON Laboratory for Space Research, Utrecht.

TABLE 1

PROGRAM STARS

HD	Name	Type	V	$B-V$	$E(B-V)$	M_{bol}	T_{eff} (K)	R_* ($R_\odot$)	$v \sin i$ (km s^{-1})	$\log \dot{M}$ ($M_\odot$ yr^{-1})	v_∞ (km s^{-1})
30614	α Cam	O9.5 Ia	4.29	0.04	0.34	−9.42	26,300	32.8	95	−5.29	2050
2905	κ Cas	B1 Ia	4.15	0.15	0.37	−8.73	21,600	35.4	62	−5.94	1500

resonance lines of α Cam. The correlation of the UV variability and the Hα and polarization variations will be discussed in a second paper.

Preliminary results of this study were published by de Jager *et al.* (1979). However, due to errors in the calibration of the *IUE* data during the first year, these results had to be reexamined when the correct intensity transformation function (ITF) became available later. This and other misfortunes have delayed the publication of the results considerably (see acknowledgments for interesting details).

II. THE *IUE* OBSERVATIONS

The two stars selected for this study of fast variations in the UV resonance lines are listed in Table 1. The data are from a compilation by Lamers (1981). The color and magnitudes (B − V and V) are from the *Bright Star Catalogue* (Hoffleit and Jaschek 1982). The excess was found by assuming $(B-V)_0 = -0.27$ for α Cam and −0.19 for κ Cas (FitzGerald 1970). These two stars were selected on the basis of their UV brightness and because spectral variations in the visual had been discovered before (Rosendahl 1973; see also Ebbets 1980). The spectral lines studied in this paper are listed in Table 2.

The observations used in this study were made with the *IUE* on 1978 September 8–10, during a continuous period of ∼72 hr. The observations were carried out alternatively by Lamers from Vilspa (8 hr shifts) and Snow from GSFC (16 hr shifts). During the first 48 hr only α Cam was observed at an average rate of one exposure per half hour. When the UV spectrum of this star did not show any appreciable variations in the quick-look plots, a second star, κ Cas, was included in the program on the third day in the hope of observing variations in at least one star. The detailed analysis presented below has shown later that the UV spectrum of the first star (α Cam) was variable, but that of the second star was not.

All spectra were taken with the high-resolution SWP camera using the wide slit. After the first few experimental observations, the optimum exposure times of 3 minutes for α Cam and 6 minutes for κ Cas were adopted. The list of observations used in this study is given in Table 3. It consists of 72 spectra of α Cam and 19 of κ Cas. The time of observation is given in

TABLE 2

LINES STUDIED

Ion	λ (Å)	f	g	ΔV (km s^{-1})	n_E/n_H[a]	n_i/n_E[b]
C IV	1548.188	0.194	2	0	3.7×10^{-4}	1.0×10^{-2}
	1550.762	0.097	2	498	3.7×10^{-4}	1.0×10^{-2}
N V	1232.808	0.152	2	0	1.1×10^{-4}	1.3×10^{-2}
	1242.796	0.076	2	965	1.1×10^{-4}	1.3×10^{-2}
Si IV	1393.755	0.528	2	0	3.5×10^{-5}	1.3×10^{-2}
	1402.770	0.264	2	1939	3.5×10^{-5}	1.3×10^{-2}

[a] From Snow and Morton 1976.
[b] From Olson and Castor (1981) O9–B0 supergiants.

day-number (September 8 = day 251) and the start of the exposure in hours and minutes. Several spectra turned out to be unreliable for this study of variability. These spectra are different from the others, in the sense that they show discrepant fluxes or line profiles in the photospheric spectrum, or a large noise. The erratic nature of these discrepant spectra indicates that they are of instrumental, rather than of stellar origin. They were omitted from further study. In several spectra this erratic behavior is only shown at ∼1380 Å. In these spectra the Si IV resonance lines near 1400 Å can not be studied. These spectra are indicated in Table 3 in the notes to the table.

After the initial calibration of all spectra in Vilspa and at GSFC, the error in the calibration intensity transfer function (ITF) was discovered. Therefore all spectra were recalibrated in 1981 at the Regional Data Analysis Facility in Boulder under the guidance of M. van Steenberg. This resulted in a homogeneous set of data in which calibration errors are minimized, and which is suitable for a study of line profile variations.

The spectra were interpolated in steps of 0.1 Å. The resolution of the calibrated spectra is ∼0.15 Å in the wavelength range between 1200 and 1550 Å. In order to minimize the influence of the noise on the spectrograms, all spectra were smoothed with the adjacent channel method, which produces a smoothed spectrum

$$\bar{F}_i = \sum_{j=-m}^{m} 2^{-2m} \binom{2m}{m+j} F_{i+j}\,, \qquad (1)$$

where F_i are the original data points in steps of 0.1 Å, $\bar{F}_i$ are the smoothed data points and the weights are the binomial coefficients with m as a smoothing parameter. After a few tests we decided that smoothing with $m = 3$ produced the best spectra; i.e., sufficient reduction of the noise with little loss of resolution. This smoothing corresponds to a profile with a FWHM of 0.3 Å or ∼65 km s^{-1} near 1300 Å, which is similar or slightly less than the values of $v \sin i$ of the two program stars.

The accuracy of the wavelength scale of the *IUE* spectra and its stability was checked by measuring the central wavelengths of a number of interstellar lines. These lines are listed in Table 4. We found that the observed wavelengths of these lines are constant within 0.04 Å, i.e., within 10 km s^{-1}, but that the measured wavelength differs from the laboratory wavelength by values up to 0.2 Å. Therefore we have corrected the wavelength scale of the *IUE* spectra in such a way that the interstellar lines are at their laboratory wavelengths. This implies a correction of +0.20 Å to the wavelength scale near the C IV lines at 1550 Å, and +0.09 Å near the N V lines of 1240 Å. For the Si IV lines at 1400 Å we adopted the mean shift of +0.15 Å. These corrections were added to the wavelength scale of the *IUE* spectra.

In order to study the profile variations, all *IUE* spectra were normalized in the same way to a "pseudocontinuum" level. This level was defined by the flux in a few windows outside the resonance lines of N V, C IV, and Si IV. These windows are

TABLE 3

THE *IUE* OBSERVATIONS

SWP (number)	Day (1978)	Time (hr)	Time (minutes)	Relative Time (minutes)	Exposure (minutes)	Remarks
			α Cam			
2520	251	1	4	0	3	1
2521	251	1	49	45	3	
2522	251	2	27	83	3	A
2524	251	3	55	171	3	
2525	251	4	26	202	3	A
2526	251	5	2	236	3	A
2527	251	5	41	277	3	A
2528	251	6	19	315	3	A
2529	251	6	56	352	3	
2530	251	7	32	388	3	A
2531	251	8	11	427	3	A
2532	251	8	45	461	3	A
2533	251	9	18	494	3	A
2535	251	10	23	559	3	
2536	251	10	55	591	3	
2537	251	11	26	622	3	
2538	251	11	58	654	3	
2539	251	12	29	685	3	
2540	251	13	8	716	3	
2541	251	13	31	747	3	
2543	251	14	37	813	3	
2544	251	15	10	846	3	
2545	251	15	41	877	3	
2546	251	16	17	913	3	B, 2
2547	251	16	49	945	3	B, 2
2548	251	17	22	978	3	B, 2
2549	251	17	52	1000	3	B
2550	251	18	23	1039	3	B
2551	251	18	53	1069	3	B, 2
2552	251	19	25	1101	3	B, 2
2553	251	19	56	1132	3	
2554	251	20	27	1163	3	B
2555	251	20	59	1195	3	
2556	251	21	37	1233	3	B
2557	251	22	12	1266	3	B
2558	251	23	2	1318	3	2
2559	251	23	38	1354	3	2
2560	252	0	16	1392	3	
2561	252	0	53	1429	3	
2562	252	2	19	1515	3	
2563	252	2	54	1550	3	
2564	252	3	28	1584	3	
2565	252	4	49	1665	3	C
2566	252	5	29	1705	3	C
2567	252	6	7	1743	3	C
2568	252	6	45	1781	3	C
			α Cam			
2569	252	7	24	1820	3	C
2570	252	8	38	1894	3	C
2571	252	9	9	1925	3	C
2572	252	9	39	1955	3	C
2573	252	10	47	2023	3	C
2574	252	11	17	2053	3	C
2575	252	11	47	2083	3	C
2576	252	12	19	2115	3	C
2577	252	13	25	2181	3	1
2580	252	15	4	2288	3	
2581	252	16	15	2351	3	
2584	252	20	15	2591	3	D, 2
2585	252	20	48	2624	3	D
2590	253	1	12	2888	3	D
2591	253	1	49	2925	3	
2594	253	4	26	3082	3	
2595	253	5	1	3117	3	
2598	253	7	29	3265	3	1
2599	253	8	8	3304	3	
2606	253	10	9	3425	3	E
2606	253	12	43	3579	3	E
2611	253	15	46	3762	3	E
2614	253	18	24	3920	3	1
2615	253	18	57	3953	3	1
2618	253	21	17	4093	3	E
2619	253	21	50	4126	3	2
			κ Cas			
2589	252	23	56	0	10	
2592	253	2	48	172	7	
2593	253	3	38	222	7	
2596	253	5	52	356	7	
2597	253	6	35	399	7	
2600	253	8	49	533	7	
2601	253	9	24	568	7	
2603	253	10	49	653	6	
2604	253	11	24	688	6	
2605	253	11	58	722	6	
2607	253	13	24	808	6	
2608	253	13	59	843	6	
2609	253	14	33	877	6	
2612	253	16	42	1006	6	
2616	253	19	42	1186	6	
2617	253	28	24	1228	6	
2628	253	22	29	1353	6	
2621	253	23	7	1391	6	
2622	253	23	43	1427	6	

REMARKS.—(1) Spectrum not studied because of unreliability. (2) Spectrum not complete in region $1370 < \lambda < 1384$ Å, i.e. not used for study of Si IV lines. A, B, C, D, and E are the time intervals, described in § III*a*.

TABLE 4

INTERSTELLAR LINES FOR CHECKING THE WAVELENGTH SCALE

Ion	λ_{lab} (Å)	λ_{obs} (Å)	$\lambda_{lab} - \lambda_{obs}$
S II	λ1253.79	1253.73 ± 0.02	0.06
	λ1259.53	1259.38 ± 0.02	0.15
Si II	λ1260.42	1260.37 ± 0.04	0.05
	λ1526.70	1526.53 ± 0.02	0.20

listed in Table 5. They were chosen because they contain no strong absorption lines, so that the mean flux in these regions could be defined accurately. The pseudocontinuum was adopted as a least-squares linear fit through these windows, with a weight factor proportional to the width of each window. This pseudo continuum provides a flux-normalization level in the wavelength ranges of the N V, C IV, and Si IV resonance lines, which has been applied to all spectra in order to allow an accurate comparison of the profiles at different times. We note that this pseudocontinuum is not the same as the true contin-

TABLE 5

Adopted Pseudocontinuum Windows Used for Normalization of the Spectra

Star	Lines	Pseudocontinuum Windows (Å)	(Å)	(Å)
α Cam	N v	1223.5–1230.5	1251.0–1253.2	1255.0–1257.6
	Si iv	1359.0–1369.0	1412.3–1418.0	1418.5–1423.5
	C iv	1512.0–1524.0	1528.0–1534.0	1562.0–1588.0
κ Cas	Si iv	1359.0–1369.0	1411.0–1415.0	1420.0–1424.0
	C iv	1512.0–1524.0	1528.0–1534.0	1562.0–1588.0

uum since the windows were not selected as the highest points in the spectrum but as relatively undisturbed spectral regions.

The resulting profiles of the N v, C iv, and Si iv lines in α Cam and of the C iv and Si iv lines in κ Cas are shown in Figures 1 and 2. These profiles are the means of all available spectra and therefore show very little noise. In both stars the lines have typical P Cygni profiles with violet-shifted absorption and redshifted emission components. Only in the Si iv lines are the two absorption components separated; in the C iv and N v lines the two absorption components of the doublets overlap one another. The cores of the lines in both stars reach the zero-intensity level except for the longward component of N v. The emission peaks of N v and Si iv are very high above the normalization level, i.e., more than twice this level, but this is obviously due to the fact that the normalization is below the actual continuum.

The edge velocities of these resonance lines, as determined by fitting the short wavelength absorption edge with a straight line and extrapolating this line to the normalization level, is for α Cam −1800 km s^{-1} for N v, −2300 km s^{-1} for C iv, and −1900 km s^{z1} for Si iv, and for κ Cas −1800 km s^{-1} for both C iv and Si iv. The large difference in the edge velocity of the three ions in α Cam is obviously due to the fact that the nor-

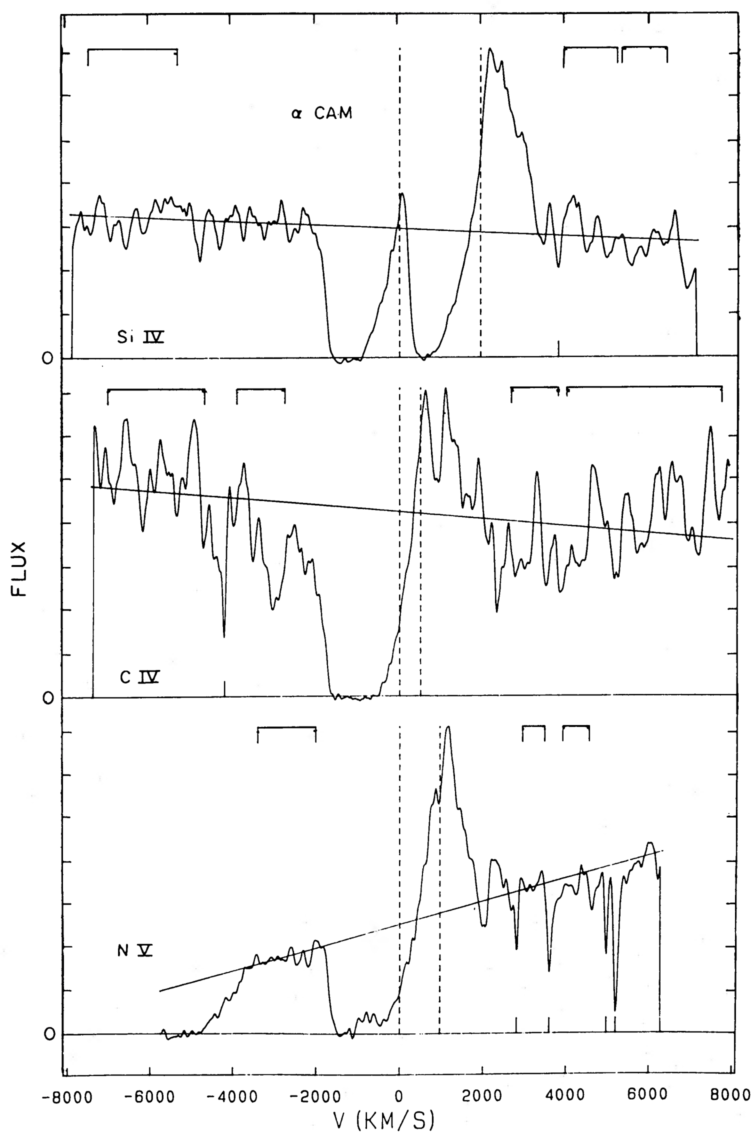

Fig. 1.—Mean line profiles in α Cam. These are the mean Si iv, C iv, and N v profiles obtained by normalization to a pseudocontinuum defined by a fit to "undisturbed" continuum wavelength windows (listed in Table 5). The dashed vertical lines indicate the rest wavelengths.

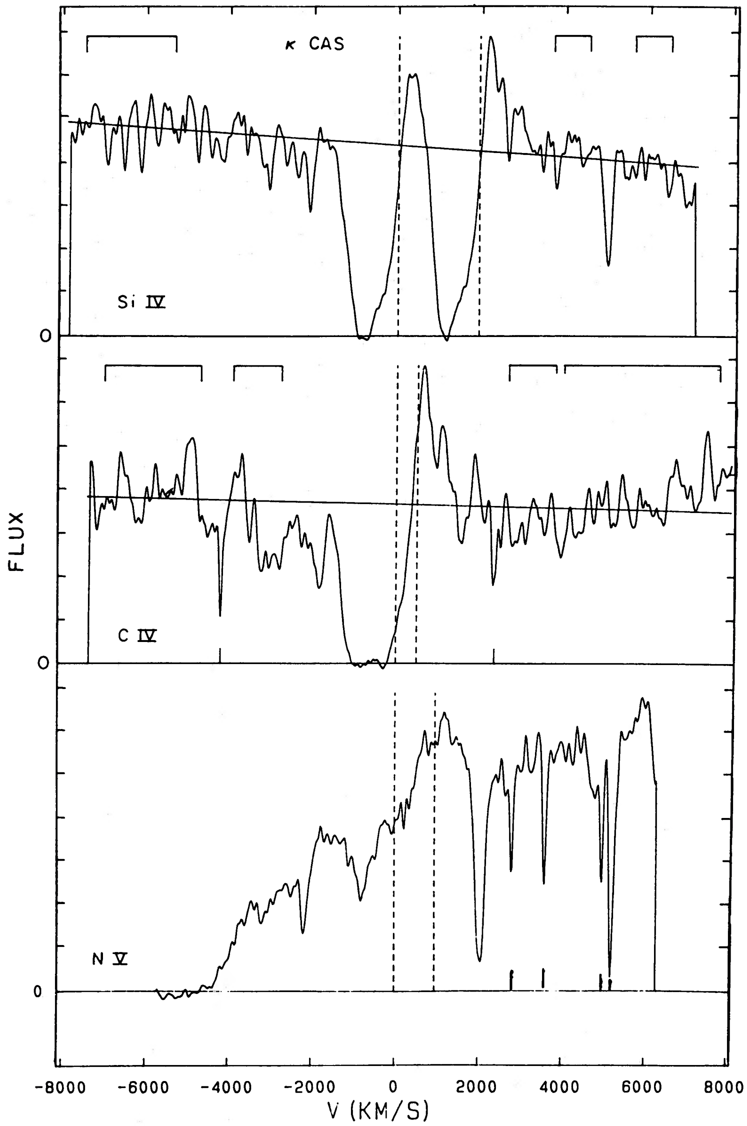

FIG. 2.—Mean line profiles in κ Cas. Same as Fig. 1

malization levels are quite different. For instance, if the normalization level of the C IV lines would have passed through the high flux point at -2500 km s^{-1} (Fig. 1*b*), the edge velocity of this line would have been reduced to -2170 km s^{-1}. Our method of determining the edge velocity does not give a reliable indication of the terminal velocity in the wind. Therefore we will adopt the values of v_∞ as listed in Table 1.

III. VARIATIONS IN THE UV RESONANCE LINES OF α CAM

a) The Criteria for Detecting Real Variations

In this section we study the observed variations in the profiles of the resonance lines of C IV, N V, and Si IV. To eliminate spurious variations due to instrumental effects and noise, the variations in the resonance lines are compared with those in the photospheric spectrum. For this purpose we have chosen "quiet" wavelength ranges outside the P Cygni profiles, the same ones as used for the determination of the pseudo continuum. This is indicated in Figures 1 and 2. We compute a noise level, σ, in this "quiet" band for each observation as the standard deviation of the difference between the individual spectrum and the mean spectrum.

The following selection criteria were adopted for the definition of real variations in the P Cygni profiles:

1. The variation must occur in two components of the same doublet or in different doublets.
2. The variation must be detected in at least two successive spectra. (This implies that we cannot study variations that occur on a time scale shorter than 1 hr.)
3. Variations that occur on a time scale of hours must reach at least 3 σ.
4. The variation must occur in the wavelength range of the P Cygni profiles.
5. The variation must occur over a wavelength range of at least 0.3 Å, which is the FWHM of the profile used for smoothing the spectra. This corresponds to $\Delta v = 50$ km s^{-1} for C IV, 73 km s^{-1} for N V, and 65 km s^{-1} for Si IV.

Using these criteria, we did not find any evidence for variations with a time scale shorter than a few hours. We did however, find strong evidence for slower variations, which will

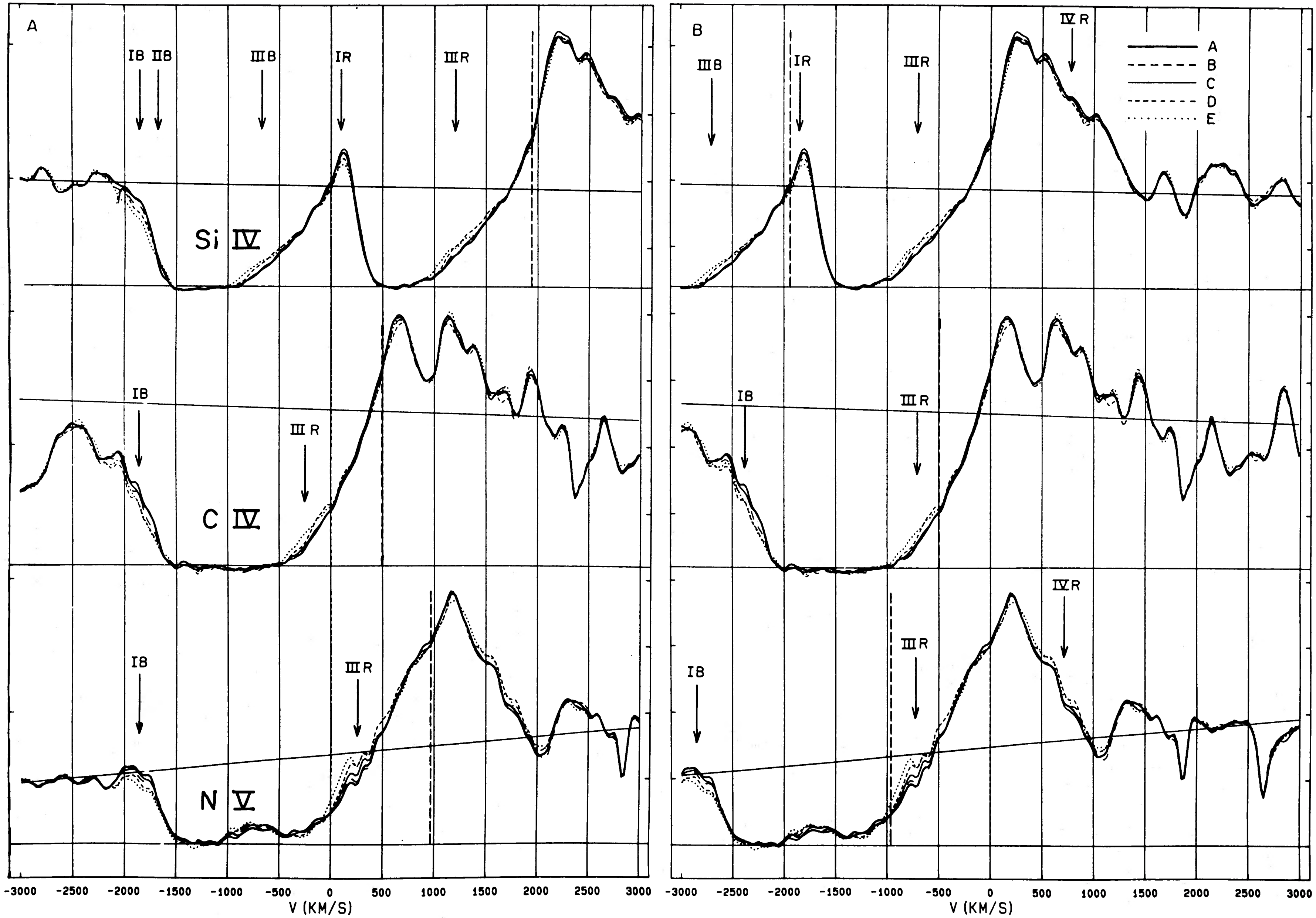

FIG. 3.—Profile variations in α Cam. The various lines (*key at upper right*) indicate the mean profiles during five 7-h intervals. (*a*) Variations on the short-wavelength side and (*b*) those on the long-wavelength side, with velocity scales based on the short-wavelength line or the doublet and the long-wavelength line, respectively. (In each case the rest position of the other component of the doublet is indicated by a dashed vertical line.) Numerical designations (Roman numerals I–IV) are used as references for the discussion in the text.

TABLE 6

TIME INTERVALS USED FOR THE STUDY OF VARIATIONS

Interval	Mid-time[a] (minutes)	Duration (minutes)
	α Cam	
A	288	452
B	1087	358
C	1877	421
D	2701	300
E	3715	671
	κ Cas	
A	131	229
B	464	219
C	788	195
D	1243	345

[a] Time for α Cam at 1978, day 251, UT = $01^h\ 04^m$; time for κ Cas is 0 at 1978, day 252, UT = $23^h\ 56^m$.

be described below. After some experimentation we found that these slower variations can be demonstrated best by binning the spectra in five time intervals of ~7 hr, called phases A, B, C, D, and E, which are regularly distributed over the total observation period. The spectra used in these phases are indicated in Table 3 by their letters. The times of the phases are given in Table 6.

b) *The Detected Variations*

The spectra during the five phases are shown in Figure 3*a*, normalized to the velocity $v = 0$ at the rest wavelength of the short-λ components. The location of the rest wavelength of the long-λ component is indicated. This rest wavelength is at $v = 498$, 965, and 1939 km s^{-1} for the C IV, N V, and Si IV doublets, respectively. To demonstrate the correspondence between variations in the blue components of the doublets and the red components, we also show the spectra normalized to the velocity $v = 0$ at the rest wavelength of the long-λ components (Fig. 3*b*). The spectra in Figure 3 show the presence of variations in several parts of the P Cygni profiles, e.g., near -1800 km s^{-1} at the short-λ side of the absorption (Fig. 3*a*) and near -700 km s^{-1} at the long-λ side of the absorption (Fig. 3*b*). The variations are indicated by I–IV (to be described below) and an "R" or "B" indicating whether the variation is due to the red (R) or the blue (B) component.

In order to demonstrate the variations more clearly, we show in Figure 4 the differential spectra relative to the one at phase A. On the left-hand side the velocity scale is normalized to the rest wavelength of the blue component, whereas in the right-hand side the velocities are relative to the rest wavelength of the red component. This makes it possible to identify the variations that occur at the same velocity in the three ions. For instance, in Figure 4*a* the variations near -1800 km s^{-1} are easily recognized for the three ions, while Figure 4*b* highlights the variations near -700, 0, and $+700$ km s^{-1}. The differential spectra outside these regions of variability provide an indication of the noise, and hence of the reliability of the observed variations.

The differential spectra in Figure 4 show that variability occurs for at least four velocities. We will indicate these by Roman numerals I, II, III, and IV in order of increasing velocity: (I) near -1800 km s^{-1} at the violet edge of the absorption, (II) near -1670 km s^{-1} at the violet edge of the absorption, and (III) near -700 km s^{-1} at the long-λ side of the absorption. For C IV and N V this variation can be seen only in the red component of the doublet, i.e., in Figure 3*a* near -200 km s^{-1} for C IV and near $+300$ km s^{-1} for N V. (IV) near $+700$ km s^{-1} in the emission components. This is best seen in Figure 4*b* for the red components of the N V doublet.

There is also some evidence for rather erratic variations near the line center (Fig. 4*b*). However, since this evidence is marginal it will not be discussed.

We will discuss the variations separately below.

i) *Variation I near* -1800 km s^{-1}

The absorption increases with time between -1700 and -2100 km s^{-1} from phase A to E. The largest variation occurs at -1800 km s^{-1}, where the Si IV line in Figure 4*a* shows a deep core in the differential spectrum. This extra absorption gets wider and stronger during the phases D and E. There is no evidence for a different behavior of the three ions; Si IV, C IV, and N V follow the same trend. Variation I is also observable in the red component of Si IV (Fig. 4*b*). Variation I cannot be observed in the red components of C IV and N V, because of the strong overlap of the doublet lines (see Fig. 3).

ii) *Variation II near* -1670 km s^{-1}

At -1670 km s^{-1} the flux in the Si IV lines has increased from phase A to phase B (i.e., within 15 hr) and remains constant from phase B to E. This phenomenon is clearly observed in both components of the Si IV doublet (Figs. 4*a* and 4*b*), and occurs only in a narrow velocity range of ~150 km s^{-1}. This effect is not seen in the C IV and N V lines. (The apparent increase in the flux at the same velocity of the red component of the N V line in Fig. 4*b* is probably due to an increase in the flux due to variation III at -700 km s^{-1} of the blue component.) The absence of this variation II in the C IV and N V lines is probably real: the profile of N V at -1670 km s^{-1} is not more strongly saturated than that of the Si IV line, and the noise is similar to that of the Si IV line.

iii) *Variation III near* -700 km s^{-1}

The flux near -700 km s^{-1} increases with time, especially from phase C to D and E, i.e. on a time scale of 30 hr. The most drastic increase is between phase C and D within 15 hr. This variation is clearly present in the blue component of Si IV and N V (Fig. 4*a*) and in the red component of the three ions. It is not found in the blue component of C IV because of saturation. There is a clear tendency for a shift to shorter wavelength of this "emission" in the differential spectra. The center of the emission is at -700 ± 30 km s^{-1} in phases C and D and at -790 ± 20 km s^{-1} in phase E. Taking the mid-times of these phases (Table 5), this shift of -90 km s^{-1} corresponds to an acceleration of -5.3 (km s^{-1})/hr or -1.5×10^2 cm s^{-2}. There is no evidence for systematically different behaviors of the Si IV, C IV, or N V lines.

iv) *Variation IV near* $+700$ km s^{-1}

In the velocity range near $+700$ km s^{-1} the differential spectra show a rather erratic behavior. The noise in the differential spectrum of C IV is too large to see any systematic trends. The red component of Si IV shows marginal evidence for an increase in flux from phase A to B and a decrease to later phases. The red component of the N V line shows an increase from phases B and C to phases D and E.

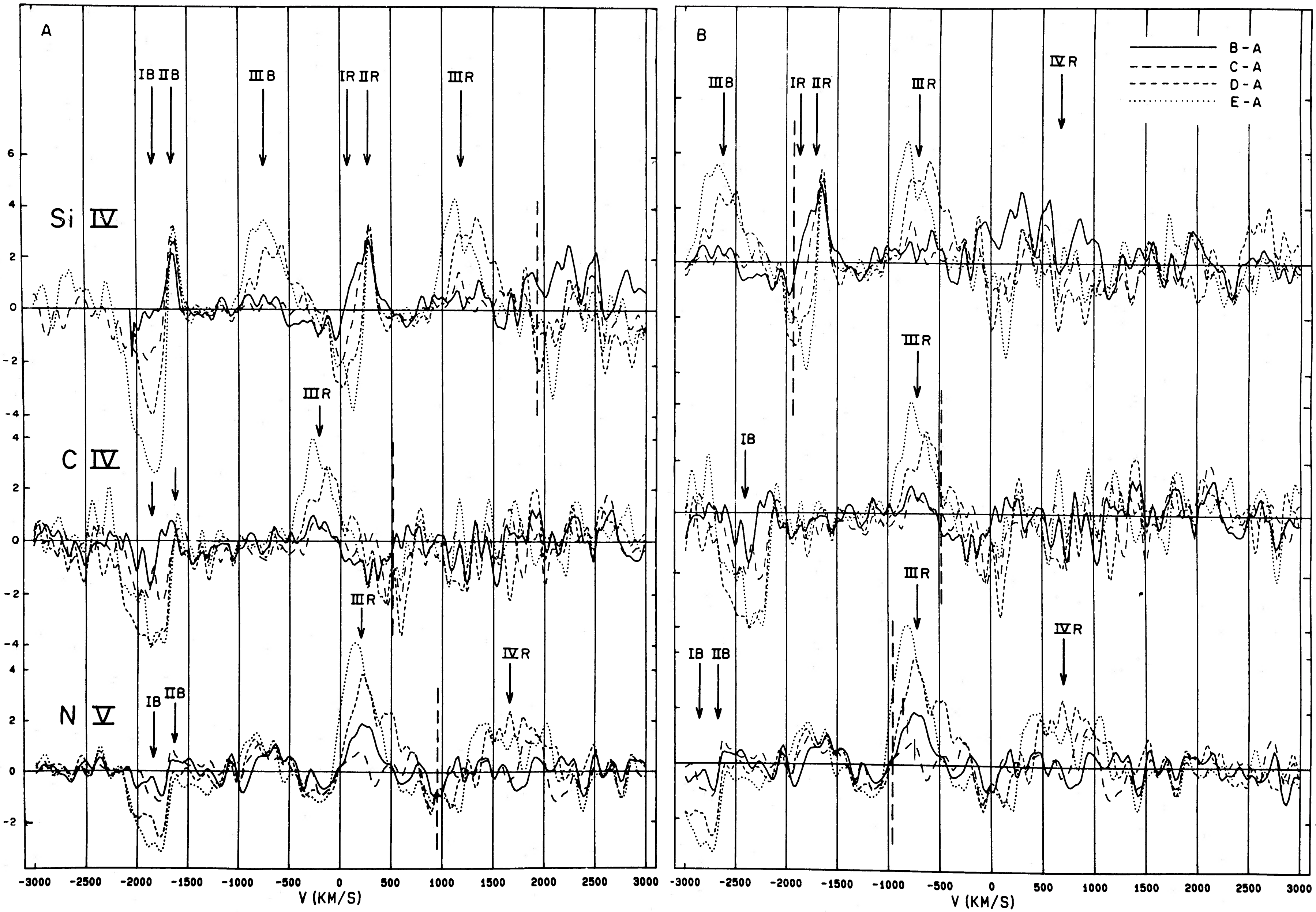

FIG. 4.—Differential spectra of α Cam in the lines of Si IV, C IV and N V. Spectrum A has been subtracted from spectra B–E (*key at upper right*) to show the variations that are seen. The vertical scale indicates the flux differences with respect to spectrum A in percentage of the pseudocontinuum. For the left-hand panel the velocity is based on the short-wavelength component of each doublet; in the right-hand panel the scale is based on the long-wavelength component. The variations I–IV which meet the stringent criteria for real variations (see § IIIa) are indicated for the blue (B) and red (R) components of the doublets.

c) *Summary of the Observed Variations*

1. At the violet edge of the absorption components the flux increases between phases A and B at -1670 km s^{-1} and decreases gradually between phases A and E in the interval $-2100 \lesssim v \leq -1700$ km s^{-1}.

2. At the red side of the absorption components the flux increases from phase A to phase E in the interval $-1000 \leq v \leq -500$ km s^{-1}. The increase is the largest between phases C and D. During this increase the central velocity of the "emission" in the differential spectra shifts from -700 to -790 km s^{-1} between phases D and E.

3. The emission of the red component at $+500 \lesssim v \lesssim +1000$ km s^{-1} decreases between phase B and the later phases in Si IV and increases in N V. This variation is less reliable than those mentioned in 1 and 2, due to the larger noise (Fig. 4*b*).

It is worth noting that variations may have occurred in the velocity range of -1000 to -1500 km s^{-1} as well. However, since the lines are saturated in this interval they cannot be detected.

IV. THE VARIATIONS AT THE VIOLET EDGE OF THE ABSORPTION COMPONENTS OF α CAM

The gradual decrease of the flux at the violet edge of the absorption component (variations I and II) indicates that the optical depth $\tau(v)$ near -1800 km s^{-1} increases with time in the three ions. This type of variation at the violet edge can be explained in two ways: either the terminal velocity of the wind increases with time, or there is an additional amount of matter at -1800 km s^{-1} due to either a shell (spherically symmetric) or a blob of gas in the line of sight to the star. The first of these two explanations is not very likely. A gradual change of the terminal velocity during the observation time would produce a shift of the steep violet edges of the lines of all three ions. This is obviously not observed. Figure 3 shows that the steep edge of the N V lines did not shift, but that the absorption increased only at -1800 km s^{-1}, just beyond the steep part of the absorption. This demonstrates that the variation in the three ions is due to the increased absorption at -1800 km s^{-1} by a blob or shell.

This blob or shell produced an extra absorption at -1670 km s^{-1} during phase A. This can be seen as a small absorption dip in the Si IV lines in Figure 3. Since this dip shifted to more negative velocity in later phases, it appears as an "emission" in the differential spectra in Figure 4, which are relative to phase A. The shift from -1670 to -1800 km s^{-1} occurred between phases A and C, with B as intermediate spectrum. During the time between phases A and C, the blob has traveled a distance of $\Delta r \approx t \times v = 1.6 \times 10^{13}$ cm $= 7.2\ R_*$. About the same distance is traveled between phases C and E, when the absorption increases in strength, but remains at about the same velocity of -1800 km s^{-1}. The differential spectra in Figure 4 shows that the "absorption" gets wider between phases C and E, i.e., it seems to extend to more negative velocities up to -2150 km s^{-1} for Si IV and N V and to -2200 for the C IV lines. (This last difference between C IV and the other two ions is most likely due to an abundance effect: the abundance of C IV ions is higher than that of Si IV and N V, as can also be seen in the stronger saturation of the C IV line and its more negative edge velocity.) This widening of the absorption indicates that the blob or shell that moved from -1670 km s^{-1} in phase A to -1800 km s^{-1} in phase C keeps increasing its velocity at later phases.

The shift in velocity of the absorption between phases A and C corresponds to an acceleration of -1.4×10^2 cm s^{-2}. Suppose that the blob or shell which produces this absorption travels with the same speed as the wind. If we adopt a velocity law of the type.

$$v(r) = v_0 + (v_\infty - v_0)(1 - R_*/r)^\beta , \tag{2}$$

with $v_\infty = 2050$ km s^{-1} and $v_0 \approx 0.01\ v_\infty \ll v_\infty$, and $\beta = 0.5$ or 1, we can compare the observed acceleration with the one predicted by equation (2). This velocity law was found to explain the UV line profiles from the winds of OB supergiants (Gathier, Lamers, and Snow 1981; Garmany *et al.* 1981). The acceleration close to the terminal velocity is

$$\frac{dv}{dt} = v\,\frac{dv}{dr} = \left[\frac{v(r)^2}{R_*}\right]\left(\frac{R_*}{r}\right)^2 \beta(1 - R_*/r)^{-1} . \tag{3}$$

Notice that the value of v_∞ does not enter in this expression. Taking $dv/dt = 1.4 \times 10^2$ cm s^{-2} and $v = 1730$ km s^{-1} we find that $r = 7.4\ R_*$ if $\beta = 0.5$ and $r = 10.2\ R_*$ if $\beta = 1$. These values apply to the mid-time between phases A and C. Since the blob traveled a distance of 7.2 R_* between phases A and C, we find from this estimate that the blob was at a distance of $5 \pm 2\ R_*$ at phase A, at $12 \pm 2\ R_*$ at phase C, and at $20 \pm 3\ R_*$ at phase E.

These distances are actually lower limits since we assume that the blob is accelerated in the same way as the quiescent wind. However, since the blob has a higher density than the quiescent wind, it is more likely that the acceleration has been slower than in the quiescent wind. (This effect is observed convincingly in the star P Cygni, which showed narrow absorption components that could be followed over a period of many months: Lamers, Korevaar, and Cassatella 1985; van Gent and Lamers 1986.)

The amount of mass in the blob is difficult to estimate. During phase A the blob or shell decreased the flux in the Si IV line at -1670 km s^{-1} by $\sim$40%. This indicates that the blob must have covered at least 40% of the line of sight to the stellar disk, or that the shell has an optical depth of $\sim$0.5. At later phases, D or E, the flux at -1800 km s^{-1} was decreased by only $\sim$20%. So at those phases the blob covered at least 20% of the stellar disk, or the shell had an optical depth of $\sim$0.2. We see from this estimate that the amount of absorbing matter in the line of sight *de*creased when the shell or blob moved outward, as expected.

We can estimate the *minimum* amount of mass needed to produce the absorption by assuming that the matter is in a blob that has a radius of 1 R_* at phase E so that it covers exactly the line of sight to the stellar disk. The blob has a minimum optical depth of 0.2 in the velocity range of -1700 to -2200 km s^{-1}, which corresponds to a minimum equivalent width W of $(W/\lambda)_{\rm min} \approx 3 \times 10^{-4}$ for the three ions. The column densities derived from this value are 1.1×10^{14} cm^{-2} for C IV, 1.8×10^{13} for N V, and 4.6×10^{13} for Si IV. Adopting the mean ionization fractions and the abundances given in Table 2 results in a minimum hydrogen column density of 3×10^{19} from C IV, 1.3×10^{20} from N V, and 1.0×10^{20} from Si IV. We adopt $N_{\rm H}({\rm min}) = 1 \times 10^{20}$ cm^{-2}. This results in a minimum mass of the blob of $M_{\rm min} = 1.8 \times 10^{-12}\ M_\odot$ if it covers exactly the line of sight to the stellar disk. This geometrical configuration, however, is very unlikely since the blob is at a distance of at least $\sim$20 R_* during phase E. A *maximum* amount of mass can be estimated by assuming that the absorption is due to a spherically symmetric shell around the star at a distance of 20 R_*. The maximum mass is 3×10^{-9} $M_\odot$. This results in the following limits for the absorbing mass

$$1.8 \times 10^{-12} \lesssim M_{\rm abs} \lesssim 3 \times 10^{-9}\ M_\odot\ . \tag{4}$$

The upper limit should be increased by a factor x^2 if the true distance of the blob is a factor x larger than the lower limit derived above.

V. THE VARIATIONS AT THE LONG WAVELENGTH SIDE OF THE ABSORPTION COMPONENT

The flux in the velocity interval $-1000 \lesssim v \lesssim -500$ km s^{-1} increased from phase A to E (variation III). Such an increase can be explained in two different ways: either there was an absorption at this velocity which decreased in time, or there was an emission which increased in time. We will consider both possibilities.

a) A Decreasing Absorption near -700 km s^{-1}

If the variations near -700 km s^{-1} are due to a decreasing absorption component, the line profiles at the various phases should be compared with the last one (E) to show this decrease. The variation can be seen best in Figure 4*b*. Since the "emissions" in the differential spectra *in*crease with time while shifting to shorter wavelengths, the differences relative to E *de*crease with time while also shifting to shorter wavelengths. The shift corresponds to an acceleration of -1.5×10^2 cm s^{-2} (see Fig. 3*b*). Suppose that the absorption is due to a blob at a distance r_b from the star which moves outward radially from the star at an angle θ relative to the line of sight to the observer. Since the blob must be in front of the disk to produce an absorption component, its velocity measured by the observer will be $v_b \cos\theta$ with $0 \le \theta \le \arcsin(R_*/r_b)$, where v_b is the velocity of the blob. If the absorption is due to a shell then $\theta = 0$ and the outward velocity of the shell is the observed velocity.

If the blob or shell were to follow the same velocity law as the quiescent wind (eq. [2]), the velocity of 700 km s^{-1} would be reached at a distance of $r \approx 1.52$ R_*, where the outward acceleration is $dv/dt = 2.7 \times 10^3$ cm s^{-2}. This predicted acceleration is 18 times larger than the observed one. If the absorption is due to a blob that moves with the wind at an angle θ, with respect to the line of sight, the expected ratio between $(dv/dt)_{\rm obs}$ and $v_{\rm obs}$, in which θ cancels, is

$$(dv/dt)/v = (v_\infty/R_*)\cdot(R_*/r_b)^2\ . \tag{5}$$

The observed values of dv/dt and v imply a distance of the blob of 6.4 R_*. At this distance, however, the velocity of the wind would be 1730 km s^{-1} and so the blob should move at an angle of 66° with respect to the observer. At this distance and angle the blob would not be observed in absorption in front of the disk. So we can conclude that the blob or shell is not moving with the same velocity law as the quiescent wind.

Suppose that the blob or shell is accelerated by radiation pressure, but that the net acceleration at any distance is a factor γ ($\gamma \le 1$) smaller than in the quiescent wind, because the density in the blob or shell is higher than in the quiescent wind. In that case the acceleration of the shell or blob is

$$\left(\frac{dv}{dt}\right)_b = \gamma\left(\frac{dv}{dt}\right)_w = \gamma v\left(\frac{dv}{dr}\right)_w \approx \gamma v_\infty^2(1 - R_*/r)R_*/r^2 \tag{6}$$

for the velocity law of equation (2) with $\beta = 1$, where v_∞ is the terminal velocity of the quiescent wind. In this expression we have neglected factors of the order $v_0/v_\infty \approx 10^{-2}$. The solution to this equation is

$$v_b(r) \approx \gamma^{1/2} v_\infty(1 - R_*/r) \tag{7}$$

and so the observed acceleration of the blob or shell as seen by the observer will be

$$-(dv/dt) \approx \cos\theta\gamma^{1/2}v_\infty v_b R_*/r_b^2$$
$$\approx v_b \cos\theta(\gamma^{1/2}v_\infty - v_b)^2/(R_*\gamma^{1/2}v_\infty) \tag{8}$$

with

$$v_b \cos\theta = -v_{\rm obs} \tag{9}$$

and the condition on θ as given above. Substituting the observed values of $dv/dt = -1.5 \times 10^2$ cm s^{-2} and $v_{\rm obs} = -700$ km s^{-1}, we find that $0 \le \theta \le 0.22$ rad and that in this narrow range of θ the corresponding values of the other parameters are $\gamma = 0.20$, $r_b = 4.3$ R_*, and $700 \le v_b \le 720$ km s^{-1} at phase D, for which we used the acceleration. This implies a distance of ~ 3 R_* at phase C.

We see that the variations at -700 km s^{-1} can be explained by a shell or blob which is accelerated ~ 0.20 times slower than the wind. This indicates that the density of the shell is $\sim (0.20)^{-1} \approx 5$ times larger than that of the wind, if the radiation pressure is produced by optically thick lines. If the radiation pressure is due to a mixture of optically thick optically thin lines, the density contrast can even be higher.

In this simple estimate we assumed that the acceleration of the blob or shell at any distance is smaller than that of the quiescent wind by the same factor γ. This is possibly an oversimplification. The interaction between the slowly accelerated shell or blob and the faster wind will eventually accelerate the material to about the same velocity as the quiescent wind. This implies that the distance derived above is a lower limit.

The amount of mass in the shell can be derived from the absorption. If we assume that the spectrum at time E represents the "normal" profile of the quiescent wind and we take spectrum C to derive the absorption at the mid-time of our observations we find equivalent widths at time C of 1.0 Å for Si IV (1394), 0.4 Å for Si IV (1403), 0.5 Å for C IV (1551), and 0.4 Å for N V (1243). This corresponds to H column densities of the blob or shell of 2×10^{20} (from Si IV), 7×10^{19} (from C IV) and 3×10^{20} (from N V). We adopt a value of 2×10^{20} H atoms cm^{-2}. In deriving this value we assumed that the blob or shell covers the whole stellar disk in the line of sight. Taking the upper limit for the distance of 3 R_* at phase C the mass of a spherical shell which can produce the absorption is estimated to be 1×10^{-10} $M_\odot$ at most. If the absorption is due to a blob which just covers the stellar disk, the mass of the blob is 4×10^{-12} $M_\odot$. This latter estimate is independent of the assumed distance of the blob. We conclude that

$$4 \times 10^{-12} \lesssim M_{\rm abs} \lesssim 1.4 \times 10^{-10}\ M_\odot\ . \tag{10}$$

The upper limit is 1.5 10^{-9} $M_\odot$ if the shell is at 10 R_*. Notice that these limits are similar to the ones derived from the absorption near -1800 km s^{-1}. This means that the absorptions near -1800 and -700 km s^{-1} can be explained by shells or blobs of comparable mass.

b) An Increasing Emission near -700 km s^{-1}

If the variations near -700 km s^{-1} are due to an emission component which increases in strength and shifts to shorter wavelengths during the observational period, the profiles at the various epochs should be compared with the profile at time A, when the emission was smallest. A shortward moving emission feature at the violet side of the rest frequency can be explained by a blob of gas, which is moving outward in a direction that makes an angle θ with the line of sight to the observer with arc sin $(R_*/r_b) \leq \theta < 90°$. If the blob is not in front of the disk, it will produce an emission component due to scattering of the stellar photons. If the blob is accelerated outward, the center of the emission will gradually move to more negative velocities.

In this case we know that the emitting gas is a blob rather than a shell, since a shell would produce an emission that is smeared out over a large frequency range from $-v_{\text{shell}}$ to $+v_{\text{shell}}$. This is not seen in our observations, in which the variable additional emission is near -700 km s^{-1}.

The amount of mass in the scattering blob can be estimated from geometrical arguments. Suppose that the blob is a sphere with a radius R_b at a distance r_b from the star. The optical depth of the blob at a frequency ν is τ_b^ν. The flux f_b^ν produced by scattering in the blob and received at the Earth is

$$f_b^\nu = (4\pi R_*^2 F_c^\nu)(\pi R_b^2/4\pi r_b^2)[1 - \exp(-\tau_b^\nu)](4\pi d^2)^{-1} . \quad (11)$$

The first factor is the stellar continuum flux, the second factor is the fraction of the stellar photons which passes through the blob, the third factor is the fraction of the photons scattered in the blob, and the fourth factor is the fraction of scattered photons which are observed at the Earth if d is the distance of the star. The height of the emission compared to the continuum is

$$f_b^\nu/F_c^\nu = 0.25(R_b/r_b)^2[1 - \exp(-\tau_b^\nu)] . \quad (12)$$

The optical depth τ_b^ν of the blob is

$$\tau_b^\nu = (\pi e^2/mc) f N_b^i \phi_\nu , \quad (13)$$

where ϕ_ν is the profile function of the absorption, f is the oscillator strength and N_b^i is the column density in the blob of the absorbing ions. This column density is related to the total number of absorbing ions in the blob by

$$N_{\text{tot}}^i \approx (\tfrac{2}{3})\pi R_b^2 N_b^i . \quad (14)$$

For optically thin blobs, $\tau_b^\nu < 1$, the equations (12), (13), and (14) yield the equivalent width of the emission relative to the continuum

$$W_\lambda/\lambda = (\tfrac{3}{8}\pi)(\pi e^2/mc)(f\lambda_0/c)R_*^{-2}(R_*/r_b)^2 N_{\text{tot}}^i . \quad (15)$$

This equation provides a lower limit of N_{tot}^i because for optically thick blobs the ratio f_b^ν/F_c^ν increases slower than N_{tot}^i.

At time E the values of W_λ/λ are 1.7×10^{-4} for Si IV (1394), 1.4×10^{-4} for Si IV (1403), 1.1×10^{-4} for C IV (1551), and $<3.5 \times 10^{-4}$ for N V (1243). The upper limit for N V is due to the fact that the location of the continuum is very uncertain. Assuming the ionization fractions and abundances in Table 2, we find the following estimates for $(R_*/r_b)^2 M_b$, where M_b is the mass of the blob: 3×10^{-12} for Si IV (1394), 5×10^{-12} for Si IV (1403), 1×10^{-12} for C IV, and $<1.5 \times 10^{-11}$ $M_\odot$ for N V (1243). Since the blob must be at a distance of at least 1.7 R_* in order to have a velocity component in the line of sight of -700 km s^{-1} and not occult the disk, we find a minimum mass of the blob of

$$M_b \gtrsim 9 \times 10^{-12} \, M_\odot . \quad (16)$$

In this case we cannot derive an upper limit for the mass of the blob.

If the variations near -700 km s^{-1} are due to emission by a scattering blob, as opposed to absorption by a blob or shell in front of the disk, it is difficult to explain the fact that the emission *in*creases with time as the blob moves outward. The predicted equivalent width of the emission is expected to vary as r_b^{-2}, i.e., it should decrease when the blob moves outward (unless the degree of ionization in the blob changes with time in favor of the observed ions). The distance traveled by the blob from phase A to E is $6.3/\cos\theta \, R_*$. So even if the blob was already at a distance of 10 R_* at time A, the equivalent width of the emission was expected to decrease by a factor 0.4 if $\theta \approx 0$. If $\theta > 0$ or the blob was closer to the star at time A, the expected decrease would be even stronger, contrary to the observed increase. This argument suggests that the variations near -700 km s^{-1} are more likely due an absorption than to an emission component.

VI. THE VARIATIONS IN THE EMISSION COMPONENTS OF Si IV AND N V

The emission component of N V in the velocity range of $+500$ to $+1000$ km s^{-1} increases by $\sim 2\%$ from phase B to phase E (Fig. 4*b*). At the same time, the red component of the C IV lines shows an irregular pattern at this velocity range, without a net increase or decrease, but the emission of the Si IV 1403 line seems to decrease with time in the range of $+500$ to $+1000$ km s^{-1}. In both the N V and the Si IV lines the largest difference with the spectrum at phase A occurs at phase C, i.e., ~ 26 hr after A. There is no evidence for a shifting of the features with time.

The profiles shown in Figure 3*b* show that the apparent absorption in the differential spectrum of the Si IV emission (Fig. 4*b*) is, in fact, due to an emission at phase A which decreases with time. This suggests that the variation of Si IV, N V and the absence of variation of C IV can be explained in the following way: A blob of gas moves away from the star at a constant velocity, v_b, e.g., the terminal velocity of the wind, i.e., 2050 km s^{-1}, at an angle θ with the line of sight to the observer such that $v_b \cos\theta \approx +700$ km s^{-1}. At phase A, when the blob is closest to the star, the ionization is such that the blob contains a significant fraction of Si IV ions, and possibly also C IV, but little N V. As time progresses and the blob moves to larger distances from the star, the degree of ionization increases such that Si IV becomes a minor constituent, the C IV content remains the same, but the N V content increases. In the real spectrum such a behavior will produce at first emission components near $+700$ km s^{-1} in the Si IV and C IV lines, and later the Si IV emission disappears and the N V emission appears. In the differential spectra, i.e., relative to phase A, this behavior will result in the development of an apparent absorption feature in Si IV, an apparent emission feature in N V, and neither absorption nor emission in C IV, in agreement with the observations.

Is there any evidence for such a variable ionization in the blob? The observations of narrow components in the spectra of many stars by Lamers, Gathier, and Snow (1982) and Prinja and Howarth (1986) show that the degree of ionization in the blobs or shells is higher than in the quiescent wind when the blobs are further away. Moreover, Prinja and Henrichs (1987) recently found narrow absorption components in the spectrum of HD 110432 which show that the degree of ionization increases with time as the shells move outward.

The amount of mass in the blob can be estimated from the equivalent widths of the blob emission by using equation (15).

The equivalent width of the Si IV 1403 emission in phase A is $\sim W_\lambda/\lambda \approx 2 \times 10^{-5}$, and the equivalent width of N V 1243 at phase E is $W_\lambda/\lambda \approx 4 \times 10^{-5}$. The distance of the blob at phase A was at least $r_b \gtrsim 5\ R_*$ since the velocity remains about constant after this phase. The Si IV/Si ratio at phase A was at least 1.3×10^{-2}, which is the value of the quiescent wind. This results in a lower limit of $M_b \gtrsim 2 \times 10^{-11}\ M_\odot$ at phase A. The distance of the blob at phase E was at least 11 R_*, i.e. 5 R_* at phase A plus 700 km s^{-1} during t(E) − t(A). The N V/N ratio at phase E was at least as high as the quiescent wind, i.e., 1.3×10^{-2}. So the mass of the blob, derived from the N V emission at phase E was $M_b \gtrsim 2 \times 10^{-10}\ M_\odot$.

We conclude that the mass of the blob which produced the variations at about +700 km s^{-1} was

$$M_b \gtrsim 2 \times 10^{-10}\ M_\odot. \tag{17}$$

VII. SUMMARY AND DISCUSSION

The *IUE* observations of α Cam, obtained during 72 hr of continuous observations in 1978 September, show variations in the C IV, Si IV and N V lines at a few-percent level. They are most clearly detectable in the differential spectra shown in Figure 4. By applying strict selection criteria (§ III*a*) we found three velocity regions (near −1800, −700, and +700 km s^{-1}) where the variations are certainly real. Variations also seem to occur at other parts of the resonance line profiles, but they are less reliable and may be due to noise in the spectra.

The absorption component at the violet edge of the resonance lines of Si IV, C IV, and N V can be explained by a blob or a shell which is at a distance of at least 3 R_* at phase A and 20 R_* at phase E. If the absorption is due to a blob which just covers the stellar disk, its mass is at least $1.8 \times 10^{-12}\ M_\odot$. If the absorption is due to a spherical shell, its mass is at least $3 \times 10^{-9}\ M_\odot$. The blob or shell has a mean acceleration of 1.4×10^2 cm s^{-2} between phases A and C and a column density of $N_{\rm H} \approx 1 \times 10^{20}$ cm^{-2}.

The variations observed on the red side of the absorption components of Si IV, C IV, and N V near −700 km s^{-1} can be explained by a blob or a shell which is at a distance of at least 3 R_* at phase C and 4 R_* at phase D. If the absorption is due to a blob that just covers the stellar disk, the mass would be at least $4 \times 10^{-12}\ M_\odot$. If the absorption is due to a spherical shell its mass is at least $1 \times 10^{-10}\ M_\odot$. The acceleration of the blob or shell is 1.5×10^2 cm s^{-2} and the column density is $N_{\rm H} \approx 2 \times 10^{20}$ cm^{-2}.

The variation in the emission components near +700 km s^{-1} can be explained by a blob of gas (*not* a shell) which moves at constant velocity in a direction away from the observer and in which the degree of ionization increases as the blob moves further away from the star. The minimum distance of this blob is estimated to be at least 5 R_* from the star at phase A and 11 R_* at phase E in order to account for the lack of acceleration. The mass of this blob must be at least $2 \times 10^{-10}\ M_\odot$.

We conclude that all the observed variations can be explained by the presence of accelerated blobs of gas. The absorptions near −2000 and −700 km s^{-1} can also be explained by shell ejections, however, such shells cannot explain the variable emission near +700 km s^{-1}. This argues for the case of blobs rather than for shells.

If the ejection is mainly in the form of blobs and if at least two blobs are observed in absorption in the line of sight to the star at distances of ~2–20 R_* during the 72 hr of observing, then blobs must be a very common characteristic of the wind of α Cam and we might expect a considerable number of blobs around the star which are not in the line of sight to the star. These should appear in emission. Why did we observe only one variable emission component? There are two reasons for this. (*a*) If the emission by scattering blobs is not variable during the 72 hr of observing time they will not be discovered in our differential spectra of Figure 4. (*b*) For the scattering emission of the blob to be measurable, the mass of the blob must be much larger than for a blob which is seen in absorption. This is due to the fact that only a small fraction of the scattered photons leave the blob in the direction to the observer. It is for this reason that the lower limit of the mass of the emitting blob, equation (17), is about a factor 10^2 larger than the lower limits of the mass of the absorbing blobs (eqs. [4] and [10]).

We discovered at least two blobs in the line of sight to the star during the 72 hr of observing. Considering the fact that we can detect the absorptions by the blobs only in the unsaturated part of the profiles, and that a large part of the absorption is saturated, we suspect that the number of blobs in the line of sight can be considerably larger. Moreover, since we used the differential spectra to detect absorptions by blobs, those blobs which are not accelerated or which do not change their optical depths will remain undetected. Therefore the number of blobs in the line of sight at any time can easily be on the order of 10 or more.

Suppose that there are ~10 blobs in the line of sight between 2 and 20 R_*, each with a column density of $N_{\rm H} \approx 2 \times 10^{20}$ (see §§ IV and V*a*), then the total column density in the form of blobs is $N_{\rm H} \approx 2 \times 10^{21}$ cm^{-2}. The total column density of the quiescent wind between 2 and 20 R_* is 1.5×10^{22} cm^{-2}. This estimate shows that a mass fraction of the order of 10^{-1} of the wind may be concentrated in blobs.

There is independent evidence for the existence of blobs in the winds of early-type supergiants. White *et al.* (1983) have reported the occurrence of X-ray spikes in the X-ray binary 4U 1700−37, which consists of an O6 f star and a compact star. They have shown that these spikes can be explained by accretion of density concentrations in the wind of the O supergiant, which have a characteristic scale of about a stellar radius in the direction perpendicular to the radial direction and a column density in the radial direction of $N_{\rm H} \lesssim 6 \times 10^{21}$ cm^{-2}.

The picture which emerges from this study is that of a "clumpy" stellar wind in which a considerable fraction of the mass, say ~10^{-1}, is in blobs. The acceleration of these blobs is smaller than that of the quiescent wind at the same distance and they are moving slower than the wind when they occur in the part of the wind where the acceleration occurs, say at $r \lesssim 5\ R_*$.

The origin of the blobs is not understood. Several mechanisms have been suggested in the literature: variable mass loss due to pulsation (maybe nonradial), streams and interacting regions in rotating magnetic stars, or instabilities which develop in the accelerating part of the wind. (For reviews see Lamers and de Loore 1987.) The results of this study may be used to set observational limits on the mass, frequency and acceleration of the blobs to test future quantitative models.

Part of this work was supported by a NASA grant to T. P. S. and an NSF grant to D. Abbott at the University of Colorado. The authors want to express their thanks to Michael van Steenberg for his efficient help in the calibration of the many spectra at the *IUE* Regional Data Analysis Facility in Boulder and to Marc Castemiller who contributed in the very early phase of the analysis. We thank the JILA Scientific Reports Office for typing the manuscript, and an unknown referee for valuable comments.

The first author is grateful to everybody involved in this study for the patience during several misfortunes which occurred in the process of this study: the discovery of an error in the *IUE* ITF when the first study was almost completed; the long illness of the first author after the final calibration was finished; and the loss of the only copies of an earlier version of the paper and most of the figures during the moving of the fourth author.

REFERENCES

De Jager, C., Lamers, H. J. G. L. M., Machetto, F., and Snow, T. P. 1979, *Astr. Ap.*, **79**, L28.
Doazan, V. 1982, in *The B Stars With and Without Emission Lines*, ed. A. B. Underhill and V. Doazan NASA SP-456.
Ebbets, D. 1980, *Ap. J.*, **235**, 97.
FitzGerald, P. M. 1970, *Astr. Ap.*, **4**, 234.
Garmany, C. D., Olson, G. L., Conti, P. S., and van Steenberg, M. E. 1981, *Ap. J.*, **250**, 660.
Gathier, R., Lamers, H. J. G. L. M., and Snow, T. P. 1981, *Ap. J.*, **247**, 173.
Henrichs, H. F. 1984, in *4th European IUE Conf.*, ed. E. Rolfe and B. Battrick, ESA SP-218, p. 43.
———. 1987, in *O, Of and Wolf-Rayet Stars*, ed. P. S. Conti and A. B. Underhill, NASA/CNRS Monograph, in press.
Hoffleit, D., and Jaschek, C. 1982, *The Bright Star Catalogue* (New Haven: Yale University Observatory.
Lamers, H. J. G. L. M. 1981, *Ap. J.*, **245**, 593.
Lamers, H. J. G. L. M., and de Loore, C. W. H., eds. 1987, *Instabilities in Luminous Early Type Stars* (Dordrecht: Reidel), Astrophysics and Space Science Library, Vol. **136**.
Lamers, H. J. G. L. M., Gathier, R., and Snow, T. P. 1982, *Ap. J.*, **258**, 186.
Lamers, H. J. G. L. M., Korevaar, P., and Cassatella, A. 1985, *Astr. Ap.*, **149**, 29.
Olson, G. L., and Castor, J. I. 1981, *Ap. J.*, **244**, 179.
Prinja, R. K., and Henrichs, H. F. 1987, in *Physics of Be Stars*, ed. A. Slettebak and T. P. Snow (Cambridge: Cambridge University Press), p. 265.
Prinja, R. K., and Howarth, I. D. 1986, *Ap. J. Suppl.*, **61**, 357.
Rosendahl, J. D. 1973, *Ap. J.*, **182**, 523.
Snow, T. P. 1977, *Ap. J.*, **217**, 760.
Snow, T. P., and Morton, D. C. 1976, *Ap. J. Suppl.*, **32**, 429.
Van Gent, R. H., and Lamers, H. J. G. L. M. 1986, *Astr. Ap.*, **158**, 335.
White, N. E., Kallman, T. R., and Swank, J. H. 1983, *Ap. J.*, **269**, 264.
York, D. G., Vidal-Madjar, A., Laurent, C., and Bonnet, R. 1977, *Ap. J. (Letters)*, **213**, L61.

HENNY J. G. L. M. LAMERS, CORNELIUS DE JAGER, and A. LANGERWERF: SRON Laboratory for Space Research, Beneluxlaan 21, 3527 HS Utrecht, The Netherlands.

THEODORE P. SNOW: University of Colorado, CASA, Campus Box 391, Boulder, CO 80309.